This is the published version of a paper published in *Physical Review Letters*.

Access to the published version may require subscription.

N.B. When citing this work, cite the original published paper.

Shock-Front Injector for High-Quality Laser-Plasma Acceleration

A. Buck,[1,2] J. Wenz,[1,2] J. Xu,[1,3] K. Khrennikov,[1] K. Schmid,[1] M. Heigoldt,[1] J. M. Mikhailova,[1]
M. Geissler,[4] B. Shen,[3] F. Krausz,[1,2] S. Karsch,[1,2,*] and L. Veisz[1,†]

[1]*Max-Planck-Insitut für Quantenoptik, Hans-Kopfermann-Strasse 1, 85748 Garching, Germany*
[2]*Ludwig-Maximilians-Universität München, Am Coulombwall 1, 85748 Garching, Germany*
[3]*State Key Laboratory of High Field Laser Physics, Shanghai Institute of Optics and Fine Mechanics,
Chinese Academy of Sciences, P. O. Box 800-211, Shanghai 201800, China*
[4]*Queen's University Belfast, Belfast BT7 1NN, United Kingdom*
(Received 4 January 2012; published 2 May 2013)

We report the generation of stable and tunable electron bunches with very low absolute energy spread ($\Delta E \approx 5$ MeV) accelerated in laser wakefields via injection and trapping at a sharp downward density jump produced by a shock front in a supersonic gas flow. The peak of the highly stable and reproducible electron energy spectrum was tuned over more than 1 order of magnitude, containing a charge of 1–100 pC and a charge per energy interval of more than 10 pC/MeV. Laser-plasma electron acceleration with Ti:sapphire lasers using this novel injection mechanism provides high-quality electron bunches tailored for applications.

Laser-driven electron acceleration activities have seen a tremendous increase over the past decade, especially since the experimental breakthrough of the first acceleration of relativistic electron bunches exhibiting monoenergetic features in their spectrum [1]. In the so-called laser wakefield acceleration (LWFA) [2], electrons are accelerated by the longitudinal electric fields of the charge density wave (plasma wave) trailing a high-intensity laser pulse through a plasma. These accelerating fields are on the order of a few 100 GV/m and thus 3–4 orders of magnitude larger than achievable in state-of-the-art radio-frequency accelerators, thereby offering a way to shrink future particle accelerators to small scale devices.

One of the important applications of the inherently few-fs long electron bunches [3,4] is currently the generation of ultrashort XUV/x-ray bursts with narrow or broad bandwidth via undulator radiation [5], Thomson backscattering [6], or betatron radiation [7,8]. Especially for narrowband x rays, a precise control of the electrons' peak energy E_{peak} and a low full width at half maximum (FWHM) energy spread ΔE are important.

These parameters are closely linked with the process of electron injection and trapping into the plasma wave, which defines the acceleration length of the particles. Self-injection via transverse wave breaking [9] offers a simple possibility to seed the accelerator; however, it has several shortcomings. The position and length of the electron injection region depends on highly nonlinear processes such as self-focusing of the laser pulse. Thus, although stable self-injection regimes have been observed [10], large fluctuations in the acceleration length and accordingly E_{peak} and ΔE are often experienced and the control over the bunch properties is very limited.

Alternative approaches for injection aiming at both the stabilization and control of the process typically prevent self-injection by choosing a laser intensity and background plasma density below the self-injection threshold, while still driving a strongly nonlinear plasma wave [11–24]. In the colliding pulse scheme, a beat wave between the main laser pulse driving the plasma wave and an additional, counterpropagating pulse heats some of the electrons at the collision point such that they gain enough momentum to be trapped [11–13]. A different scheme is ionization injection, where gas mixtures with different ionization intensity thresholds are used to inject electrons that are liberated from the core in the correct phase of the plasma wave; however, only very broad electron spectra are achieved with this technique [14,15]. Modulation of the plasma density profile offers a third way to control electron trapping. In slow density downramps, the plasma wavelength λ_p, given in the nonrelativistic limit [16] as $\lambda_p = 2\pi c \sqrt{\epsilon_0 m_e / n_e e^2}$, where e and m_e are the electron charge and mass, n_e the background electron density, ϵ_0 the vacuum permittivity, and c the vacuum speed of light, increases with propagation through the plasma. Thus, the phase velocity of the plasma wave behind the laser pulse is reduced; i.e., the electron density maxima propagate with a reduced velocity. Thus, a larger portion of the plasma wave electrons are faster than the local phase velocity and can propagate into the accelerating part and be trapped. This has been demonstrated experimentally for mildly relativistic electron bunches with low absolute energy spread [17]. Recently, it was shown that highly relativistic electron bunches can also be generated with high stability in this scheme, however, with $\Delta E \sim 50$ MeV and $\Delta E / E \approx 20\%$–$50\%$, because the injection process extended over a certain period [18].

In contrast to slow downramps, sharp downward density jumps with a scale length of λ_p or even shorter enable a fundamentally different injection process [20–24]. To understand and illustrate the process, we have performed three-dimensional particle-in-cell (PIC) simulations with the codes ILLUMINATION [25] and VORPAL [26] using the measured density profile and parameters matching the presented experiments. Figure 1(a) shows the longitudinal density profile with the step and Figs. 1(b)–1(d) lineouts of the electron density distribution in the plasma wave at three different time frames during the propagation of the laser pulse through the plasma [27]. To illustrate the injection effect, only carefully selected lineouts of the 3D simulation are plotted. In the high density part (n_1) before the transition, the laser excites a nonlinear plasma wave with its distinct peaks in the electron density separated by $\lambda_{p,1}$. Here, the nonlinearity of the plasma wave is below the threshold for self-injection. Due to the sharp transition, the first peak is still in the same distance behind the laser pulse right after it has entered the region with lower density n_2. Here, the plasma wave forms again with $\lambda_{p,2} > \lambda_{p,1}$ and a new electron density maximum evolves behind the one that is left over from before the transition [Fig. 1(d)]. Thus, the

electrons from the initial wave are injected into the accelerating phase, where some of them are trapped and accelerated. Our simulations show that the injection process starts to degrade for longer transition widths and ceases completely for $> \lambda_p$. Due to the extremely rapid injection, all electrons are injected at the same position and have the same acceleration length leading to small ΔE. Simulations indicate that in the second bucket the electrons are injected more to the front; thus, they dephase much sooner and also defocus at the electron density maximum at the back of the first oscillation. Thus, these electrons are not detected in the experiment. During this injection mechanism, the plasma wave never reaches the classical wave-breaking limit, where self-injection takes place.

While this scheme has been studied theoretically [20,21] in great detail, first experimental attempts, where the transition was created by a second, perpendicularly propagating laser pulse arriving before the main pulse, have not been able to produce stable, monoenergetic electron bunches [22,23], possibly due to the transition being longer than λ_p. Recently, a new approach to produce these sharp transitions by shock fronts in supersonic flows has been presented [24]. While it was demonstrated that this controlled injection improves the accelerator output significantly compared to the self-injection scheme, these experiments have been performed with sub-10-fs laser pulses with low pulse energy limiting the achievable electron energy, bunch charge, and tunability.

In this Letter, we present the successful realization of the described scheme, now producing stable electron bunches with higher charge and widely tunable energy. To this end, we used ATLAS, a Ti:sapphire laser delivering pulses with 28 fs and an on-target energy of 770 mJ. A FWHM spot size of 13.5 μm and an intensity of 8.5×10^{18} W/cm^2 ($a_0 = 2.0$) is reached with a $f/15$ focusing geometry, taking losses due to residual phase front distortions into account. The experimental setup is shown in Fig. 2. The ATLAS pulses are focused into the He gas target. As in
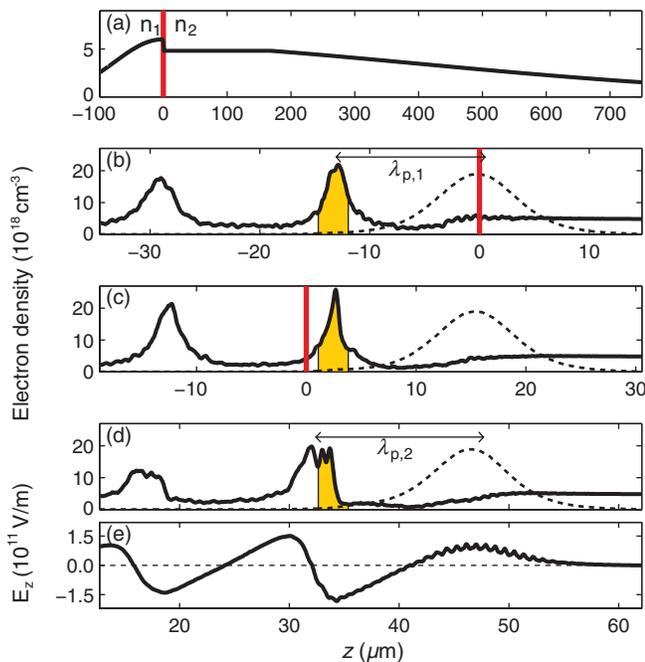

FIG. 1 (color). PIC simulation with ILLUMINATION with parameters closely matching the experimental conditions for Fig. 4(c). (a) Longitudinal background electron density profile of the target including shock front (red line). (b)–(d) Lineouts of the electron density (solid line) at different time steps. The laser pulse (dashed line) is (b) $z = 0$ μm, (c) $z = 17$ μm, and (d) $z = 46$ μm after the sharp density transition (red line). The marked area is the density maximum at the end of the first plasma oscillation that is injected after the transition. (e) Longitudinal electric field for (d).
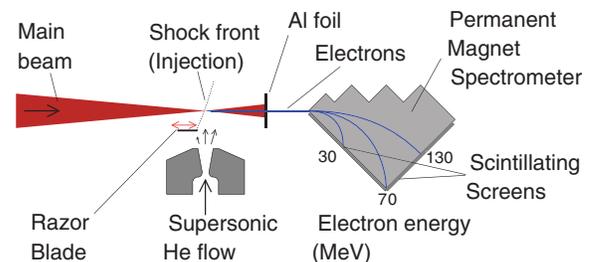

FIG. 2 (color). Experimental setup. The laser pulses are focused by an off-axis parabola into the He jet with the sharp density transition at the shock front. The razor blade generating the shock front is adjusted to control the injection position. The laser light is blocked by a 10 μm thin Al foil after the interaction, while the relativistic electrons propagate to the electron spectrometer for detection.
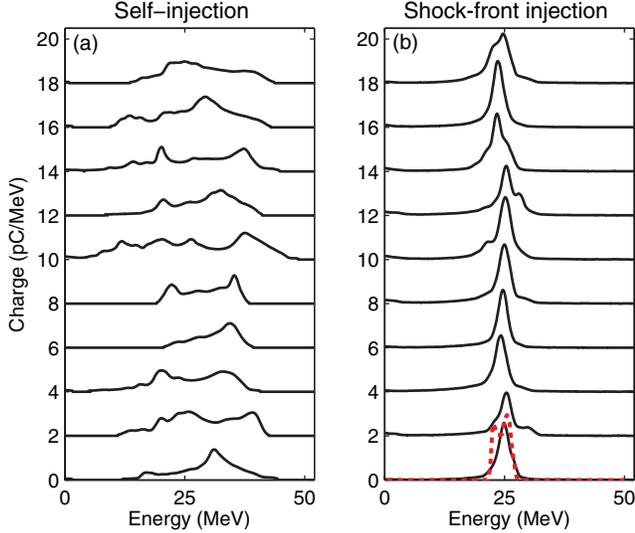
FIG. 3 (color online). Integrated lineouts of the electron spectrometer of ten consecutive shots with self-injection (a) and controlled injection with the shock front (b) for comparison. The dashed red line shows an energy spectrum from a VORPAL PIC simulation with parameters matching the experimental conditions.

Schmid *et al.* [24], a razor blade is placed as an obstacle in a supersonic flow produced by a de Laval nozzle. Due to the supersonic flow speed, the gas flow has to adapt locally to the distortion; i.e., a shock front is formed in the gas, which has a higher density n_1 than the gas in the undisturbed part of the jet (here: $n_2 \approx 0.6 n_1$). At the edge of the shock front, a sharp density transition develops, which is

used for electron injection. The electron energy spectrum is recorded by a high resolution, absolutely calibrated permanent magnet spectrometer [28].

Figure 3 shows a comparison of the accelerator output of consecutive laser shots utilizing the conventional self-injection and the new controlled injection method. In the experiment, electrons have been first accelerated via self-injection without the razor blade at a background electron density of $n_e = 1.2 \times 10^{19}$ cm^{-3}. Statistics of 500 shots after parameter optimization showed an injection probability of 93%, $E_{\text{peak}} = 27$ MeV, and an absolute FHWM energy spread of $\Delta E = 21$ MeV. Subsequently, the background density was reduced to $n_e = 0.6 \times 10^{19}$ cm^{-3}, where the injection probability dropped to zero and no accelerated electrons could be detected. Upon moving the razor blade into the flow and creating the sharp density transition, stable electron bunches with $E_{\text{peak}} = 25$ MeV and $\Delta E = 3$ MeV appeared on the detector with a probability of 99%. The absence of any lower energy electrons in the controlled injection case proves that all accelerated electrons are injected at the density transition.

The location of the density transition as well as the total acceleration length and thus also the final electron energy are precisely tunable by varying the position of the razor blade. Figure 4 shows six different runs with the same laser parameters, where the setup was tuned to produce different electron energies [27]. The statistics (Table I) show that $\Delta E \approx 5$–6 MeV is constant for all runs; i.e., the absolute energy spread is defined by the injection and conserved during the acceleration. Accordingly, the relative energy spread is reduced for higher energies. Figure 4(g) shows
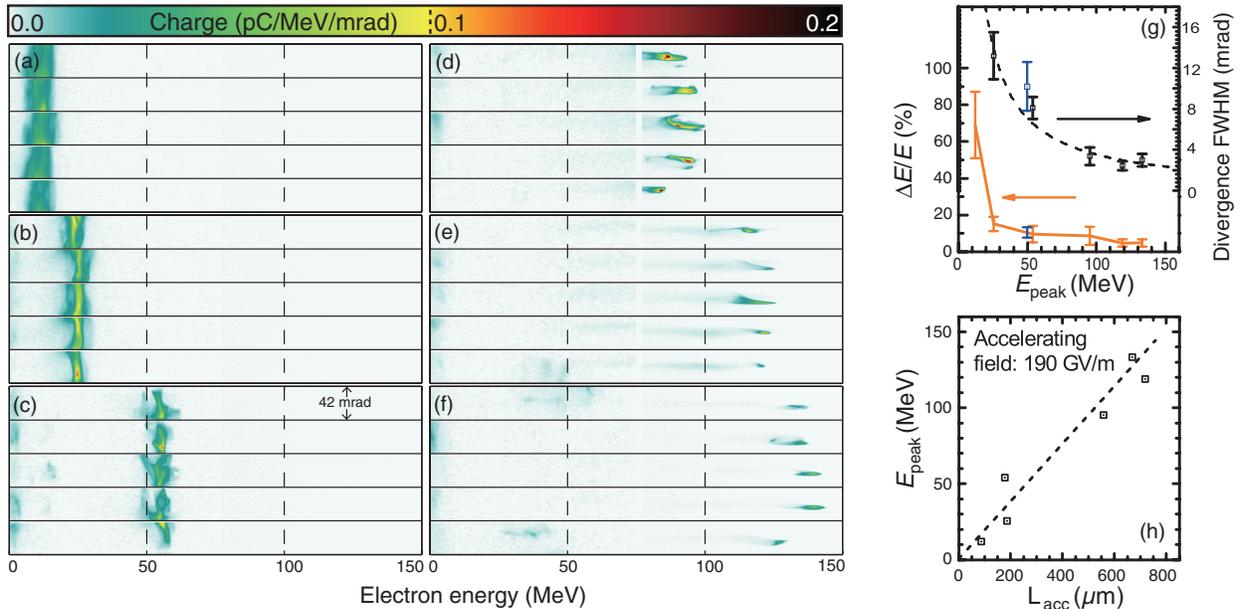

FIG. 4 (color). (a)–(f) Spectrometer images of five consecutive shots for each of six different runs where the accelerator was tuned to different energies. (g) Relative energy spread and divergence for all runs. The high charge run presented in Fig. 5 is plotted for comparison (blue). (h) Estimated acceleration length and peak energy.

TABLE I.   Comparison of shock front injection runs.

E_{peak} (MeV)	ΔE (MeV)	Q_{peak} (pC)	n_e (cm^{-3})
12.1 ± 1.3	8.3 ± 2.2	8.5 ± 4.3	2.5×10^{18}
25.6 ± 1.0	3.9 ± 1.0	6.5 ± 2.5	6.0×10^{18}
54.0 ± 1.3	5.2 ± 2.4	6.2 ± 2.5	5.0×10^{18}
95.3 ± 4.8	8.3 ± 4.7	6.0 ± 3.8	2.8×10^{18}
119.0 ± 4.8	5.6 ± 2.4	1.5 ± 0.8	2.7×10^{18}
133.3 ± 7.2	6.5 ± 2.7	1.2 ± 1.0	3.3×10^{18}
49.8 ± 2.6	5.3 ± 1.4	90 ± 30	1.5×10^{18}

the FWHM divergence for all runs. The data are in good agreement with the $1/\gamma$ fit, proving that not only the absolute energy spread, but also the normalized transverse emittance is approximately conserved during the acceleration and determined only by the injection process, as also observed by Sears *et al.* [29].

Tuning of the injection position also enables a measurement of the accelerating field. The termination of the acceleration has been estimated as the location where the plasma density has dropped to 80% of the maximum value in the plateau n_2. This assumption does not affect the accelerating gradient. Although the measurements in Fig. 4 have been performed at different densities, an average accelerating field of 190 GV/m is derived, which
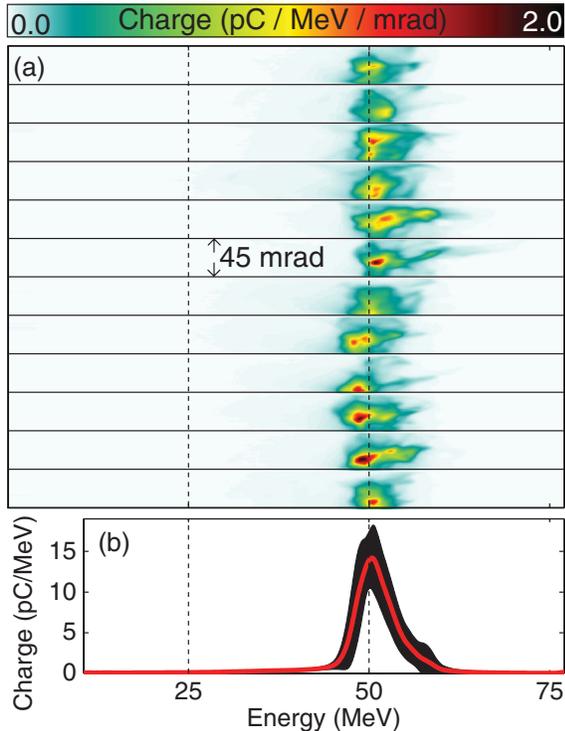

FIG. 5 (color).   High-charge shots with the upgraded laser (1200 mJ). (a) Electron detector images of twelve consecutive laser shots with a bunch charge of $Q = (90 \pm 30)$ pC. (b) Average integrated lineout (red line) and root-mean-square (black area) of these shots.

matches the value expected from the nonrelativistic, cold wave-breaking limit of 185 GV/m for the average density of $n_{e,avg} \approx 3.7 \times 10^{18}$ cm^{-3} [30].

A laser upgrade close to the end of the experimental campaign enabled us to repeat the measurements with a higher on-target pulse energy of 1200 mJ, again taking all losses into account, reaching $a_0 = 2.5$. With the new laser parameters, a significant increase in the accelerated charge has been observed. Figure 5 shows a stable run, where the accelerator was tuned to 50 MeV [27]. Here, the charge could be increased strongly, while keeping the energy spread at $\Delta E \approx 5$ MeV. Thus, a charge per energy interval of more than 10 pC/MeV was reached, which is the highest reported value to our knowledge for stable, highly relativistic electron bunches. Beam-loading effects [31], i.e., a reduction of the accelerating field and increased energy spread for high charges, have not been observed here, which is probably due to the low plasma density of $\approx 1.5 \times 10^{18}$ cm^{-3} in this run. In general, electrons have been accelerated with stable parameters from shot to shot over an extended range (up to 200 MeV) and obtaining significantly higher charges compared to the results with lower laser pulse energy.

In conclusion, we have shown that shock-front injection, i.e., electron trapping at sharp density jumps produced by a shock front in supersonic flows, offers a very powerful, yet simple method to inject electrons into laser-driven wakefields. The results demonstrate that not only the reproducibility, stability, and tunability is improved strongly compared to self-injection experiments, but also that the absolute energy spread of $\Delta E \approx 5$ MeV is significantly lower compared to other injection methods producing highly relativistic electron bunches. The charge per energy interval, an important number for all future applications such as undulator radiation, was increased strongly due to the narrow bandwidth and the bunch charge being on the order of 1–100 pC. The maximum electron energy was limited around 150–200 MeV due to limitations of the setup in the present experiment; however, several 100 MeV as already shown in other experiments with similar laser parameters are expected with improvements being currently under way. Thus, relative energy spreads below 1% FWHM are within reach.

*stefan.karsch@mpq.mpg.de
†laszlo.veisz@mpq.mpg.de

[1] S. P. D. Mangles, C. D. Murphy, Z. Najmudin, A. G. R. Thomas, J. L. Collier, A. E. Dangor, E. J. Divall, P. S. Foster, J. G. Gallacher, C. J. Hooker, D. A. Jaroszynski, A. J. Langley, W. B. Mori, P. A. Norreys, F. S. Tsung,

R. Viskup, B. R. Walton, and K. Krushelnick, Nature (London) **431,** 535 (2004); C. G. R. Geddes, C. Toth, J. van Tilborg, E. Esarey, C. B. Schroeder, D. Bruhwiler, C. Nieter, J. Cary, and W. P. Leemans, Nature (London) **431,** 538 (2004); J. Faure, Y. Glinec, A. Pukhov, S. Kiselev, S. Gordienko, E. Lefebvre, J.-P. Rousseau, F. Burgy, and V. Malka, Nature (London) **431,** 541 (2004).

[2] T. Tajima and J. M. Dawson, Phys. Rev. Lett. **43,** 267 (1979).

[3] O. Lundh, J. Lim, C. Rechatin, L. Ammoura, A. Ben-Ismail, X. Davoine, G. Gallot, J.-P. Goddet, E. Lefebvre, V. Malka, and J. Faure, Nat. Phys. **7,** 219 (2011).

[4] A. Buck, M. Nicolai, K. Schmid, C. M. S. Sears, A. Sävert, J. M. Mikhailova, F. Krausz, M. C. Kaluza, and L. Veisz, Nat. Phys. **7,** 543 (2011).

[5] M. Fuchs, R. Weingartner, A. Popp, Z. Major, S. Becker, J. Osterhoff, I. Cortrie, B. Zeitler, R. Hörlein, G. D. Tsakiris, U. Schramm, T. P. Rowlands-Rees, S. M. Hooker, D. Habs, F. Krausz, S. Karsch, and F. Grüner, Nat. Phys. **5,** 826 (2009).

[6] H. Schwoerer, B. Liesfeld, H.-P. Schlenvoigt, K.-U. Amthor, and R. Sauerbrey, Phys. Rev. Lett. **96,** 014802 (2006).

[7] S. Kneip *et al.*, Nat. Phys. **6,** 980 (2010).

[8] S. Cipiccia *et al.*, Nat. Phys. **7,** 867 (2011).

[9] S. V. Bulanov, F. Pegoraro, A. M. Pukhov, and A. S. Sakharov, Phys. Rev. Lett. **78,** 4205 (1997).

[10] J. Osterhoff, A. Popp, Z. Major, B. Marx, T. P. Rowlands-Rees, M. Fuchs, M. Geissler, R. Hörlein, B. Hidding, S. Becker, E. A. Peralta, U. Schramm, F. Grüner, D. Habs, F. Krausz, S. M. Hooker, and S. Karsch, Phys. Rev. Lett. **101,** 085002 (2008).

[11] E. Esarey, R. F. Hubbard, W. P. Leemans, A. Ting, and P. Sprangle, Phys. Rev. Lett. **79,** 2682 (1997).

[12] J. Faure, C. Rechatin, A. Norlin, A. Lifschitz, Y. Glinec, and V. Malka, Nature (London) **444,** 737 (2006).

[13] C. Rechatin, J. Faure, A. Ben-Ismail, J. Lim, R. Fitour, A. Specka, H. Videau, A. Tafzi, F. Burgy, and V. Malka, Phys. Rev. Lett. **102,** 164801 (2009).

[14] A. Pak, K. A. Marsh, S. F. Martins, W. Lu, W. B. Mori, and C. Joshi, Phys. Rev. Lett. **104,** 025003 (2010).

[15] C. McGuffey, A. G. R. Thomas, W. Schumaker, T. Matsuoka, V. Chvykov, F. J. Dollar, G. Kalintchenko, V. Yanovsky, A. Maksimchuk, K. Krushelnick,

[16] V. Y. Bychenkov, I. V. Glazyrin, and A. V. Karpeev, Phys. Rev. Lett. **104,** 025004 (2010).

[16] S. Bulanov, N. Naumova, F. Pegoraro, and J. Sakai, Phys. Rev. E **58,** R5257 (1998).

[17] C. G. R. Geddes, K. Nakamura, G. R. Plateau, C. Toth, E. Cormier-Michel, E. Esarey, C. B. Schroeder, J. R. Cary, and W. P. Leemans, Phys. Rev. Lett. **100,** 215004 (2008).

[18] A. J. Gonsalves, K. Nakamura, C. Lin, D. Panasenko, S. Shiraishi, T. Sokollik, C. Benedetti, C. B. Schroeder, C. G. R. Geddes, J. van Tilborg, J. Osterhoff, E. Esarey, C. Toth, and W. P. Leemans, Nat. Phys. **7,** 862 (2011).

[19] B. Shen, Y. Li, K. Nemeth, H. Shang, Y.-c. Chae, R. Soliday, R. Crowell, E. Frank, W. Gropp, and J. Cary, Phys. Plasmas **14,** 053115 (2007).

[20] H. Suk, N. Barov, J. B. Rosenzweig, and E. Esarey, Phys. Rev. Lett. **86,** 1011 (2001).

[21] P. Tomassini, M. Galimberti, A. Giulietti, D. Giulietti, L. A. Gizzi, L. Labate, and F. Pegoraro, Phys. Rev. ST Accel. Beams **6,** 121301 (2003).

[22] J. U. Kim, N. Hafz, and H. Suk, Phys. Rev. E **69,** 026409 (2004).

[23] T.-Y. Chien, C.-L. Chang, C.-H. Lee, J.-Y. Lin, J. Wang, and S.-Y. Chen, Phys. Rev. Lett. **94,** 115003 (2005).

[24] K. Schmid, A. Buck, C. M. S. Sears, J. M. Mikhailova, R. Tautz, D. Herrmann, M. Geissler, F. Krausz, and L. Veisz, Phys. Rev. ST Accel. Beams **13,** 091301 (2010).

[25] M. Geissler, J. Schreiber, and J. Meyer-ter Vehn, New J. Phys. **8,** 186 (2006).

[26] C. Nieter and J. R. Cary, J. Comput. Phys. **196,** 448 (2004).

[27] See Supplemental Material at http://link.aps.org/supplemental/10.1103/PhysRevLett.110.185006 for additional information about experimental parameters and particle-in-cell (PIC) simulations.

[28] C. M. S. Sears, S. Benavides Cuevas, U. Schramm, K. Schmid, A. Buck, D. Habs, F. Krausz, and L. Veisz, Rev. Sci. Instrum. **81,** 073304 (2010).

[29] C. M. S. Sears, A. Buck, K. Schmid, J. Mikhailova, F. Krausz, and L. Veisz, Phys. Rev. ST Accel. Beams **13,** 092803 (2010).

[30] E. Esarey, C. B. Schroeder, and W. P. Leemans, Rev. Mod. Phys. **81,** 1229 (2009).

[31] C. Rechatin, X. Davoine, A. Lifschitz, A. B. Ismail, J. Lim, E. Lefebvre, J. Faure, and V. Malka, Phys. Rev. Lett. **103,** 194804 (2009).